



Article

# Advanced State-of-Health Estimation for Lithium-Ion Batteries Using Multi-Feature Fusion and KAN-LSTM Hybrid Model

Zhao Zhang <sup>1,\*</sup> , Runrun Zhang <sup>2,\*</sup>, Xin Liu <sup>3</sup>, Chaolong Zhang <sup>1,\*</sup> , Gengzhi Sun <sup>2</sup>, Yujie Zhou <sup>1</sup>, Zhong Yang <sup>1</sup>, Xuming Liu <sup>1</sup>, Shi Chen <sup>1</sup>, Xinyu Dong <sup>4</sup>, Pengyu Jiang <sup>5</sup> and Zhexuan Sun <sup>3</sup>

<sup>1</sup> College of Intelligent Science and Control Engineering, Jinling Institute of Technology, Nanjing 211169, China; [yujay\\_zhou@126.com](mailto:yujay_zhou@126.com) (Y.Z.); [yz@jit.edu.cn](mailto:yz@jit.edu.cn) (Z.Y.); [lxm@jit.edu.cn](mailto:lxm@jit.edu.cn) (X.L.); [chenshi@jit.edu.cn](mailto:chenshi@jit.edu.cn) (S.C.)

<sup>2</sup> Institute of Advanced Materials, Nanjing Tech University, Nanjing 210009, China; [iamgzsun@njtech.edu.cn](mailto:iamgzsun@njtech.edu.cn)

<sup>3</sup> College of Intelligent Systems Science and Engineering, Harbin Engineering University, Harbin 150001, China; [xinliu1224@hrbeu.edu.cn](mailto:xinliu1224@hrbeu.edu.cn) (X.L.); [sunzhexuan@hrbeu.edu.cn](mailto:sunzhexuan@hrbeu.edu.cn) (Z.S.)

<sup>4</sup> College of Intelligent Science and Control Engineering, Shanghai Maritime University, Shanghai 201306, China; [202430510014@stu.shmtu.edu.cn](mailto:202430510014@stu.shmtu.edu.cn)

<sup>5</sup> College of Automation & College of Artificial Intelligence, Nanjing University of Posts and Telecommunications, Nanjing 210023, China; [1224056125@njupt.edu.cn](mailto:1224056125@njupt.edu.cn)

\* Correspondence: [zhang888@jit.edu.cn](mailto:zhang888@jit.edu.cn) (Z.Z.); [202461222188@njtech.edu.cn](mailto:202461222188@njtech.edu.cn) (R.Z.); [zhangchaolong@jit.edu.cn](mailto:zhangchaolong@jit.edu.cn) (C.Z.)

**Abstract:** Accurate assessment of battery State of Health (SOH) is crucial for the safe and efficient operation of electric vehicles (EVs), which play a significant role in reducing reliance on non-renewable energy sources. This study introduces a novel SOH estimation method combining Kolmogorov–Arnold Networks (KAN) and Long Short-Term Memory (LSTM) networks. The method is based on fully charged battery characteristics, extracting key parameters such as voltage, temperature, and charging data collected during cycles. Validation was conducted under a temperature range of 10 °C to 30 °C and different charge–discharge current rates. Notably, temperature variations were primarily caused by seasonal changes, enabling the experiments to more realistically simulate the battery’s performance in real-world applications. By enhancing dynamic modeling capabilities and capturing long-term temporal associations, experimental results demonstrate that the method achieves highly accurate SOH estimation under various charging conditions, with low mean absolute error (MAE) and root mean square error (RMSE) values and a coefficient of determination ( $R^2$ ) exceeding 97%, significantly improving prediction accuracy and efficiency.

**Keywords:** lithium-ion battery; multi-feature; KAN-LSTM; state of health



**Citation:** Zhang, Z.; Zhang, R.; Liu, X.; Zhang, C.; Sun, G.; Zhou, Y.; Yang, Z.; Liu, X.; Chen, S.; Dong, X.; et al. Advanced State-of-Health Estimation for Lithium-Ion Batteries Using Multi-Feature Fusion and KAN-LSTM Hybrid Model. *Batteries* **2024**, *10*, 433. <https://doi.org/10.3390/batteries10120433>

Academic Editor: Rodolfo Dufo-López

Received: 24 October 2024

Revised: 25 November 2024

Accepted: 28 November 2024

Published: 6 December 2024



**Copyright:** © 2024 by the authors. Licensee MDPI, Basel, Switzerland. This article is an open access article distributed under the terms and conditions of the Creative Commons Attribution (CC BY) license (<https://creativecommons.org/licenses/by/4.0/>).

## 1. Introduction

As worldwide interest in sustainable and eco-conscious transportation solutions increases, lithium-ion batteries have become crucial in electric vehicles, smart grids, and portable electronics because of their high energy storage capacity, long-lasting performance, and eco-friendly benefits [1,2]. However, over time, lithium batteries inevitably experience capacity degradation and increased internal resistance, which can lead to reduced performance, decreased battery life, and potential safety risks [3–5]. As a result, accurate monitoring and forecasting of the SOH of lithium batteries are vital for improving battery management systems and prolonging battery life [6–8]. Recently, researchers proposed many ways to forecast the SOH of lithium batteries, which are mostly data-driven and model-based.

Conventional SOH estimation techniques typically depend on either the equivalent circuit model (ECM) or the electrochemical model (EM) of batteries. Among these methods, the ECM is commonly used to estimate the SOH of the lithium-ion battery. Amir et al. explored the degradation behavior of lithium batteries using the 2-RC model, showing

that this model accounts for both time-dependent factors and temperature effects on battery performance. Compared to the traditional 1-RC model, the 2-RC model enhances prediction accuracy, although it increases computational complexity [9]. In contrast, A comprehensive ECM model that considers the effects of temperature, SOC, and SOH on the model was proposed by Tran et al. Their findings showed that while polarization capacitance drops, ohmic resistance and polarization resistance both rise with decreasing SOH. This model, recognized for its simplicity and accuracy, is well-suited for contemporary battery management systems [10].

Electrochemical modeling (EM) has received increased interest in the past few years since its capability to precisely depict the physical and chemical processes occurring within lithium batteries. Xiong et al. developed an aging state identification approach based on an electrochemical model, which includes a series of complex mathematical equations to represent various physical and chemical processes in the battery, such as ion diffusion, charge conservation, and electrochemical reactions. These equations encompass both the electrolyte and solid phase dynamics and are solved using numerical methods like finite analysis to handle the coupled partial differential equations (PDEs) inherent in the model [11]. Through numerical simulations and optimization techniques, the model parameters were accurately identified. Experimental validation of this model demonstrated a voltage discrepancy within 50 mV and an estimation error for the health state below 3% [12].

Beyond traditional methods, several innovative approaches have emerged in recent years, showing significant potential for lithium battery SOH prediction. For instance, single-particle models (SP) and incremental capacity analysis offer fresh insights into SOH forecasting. Li et al. introduced a single-particle degradation model, which integrates the formation of the solid electrolyte interface (SEI) layer and crack propagation phenomena. This model is designed to rapidly predict capacity degradation with high accuracy, making it highly suitable for online estimation applications [13]. Similarly, Maures et al. proposed an SOH diagnostic method centered on incremental capacity (IC) peak tracking tailored for scenarios involving high C-rates. Their findings demonstrated a strong correlation between IC peak shifts and SOH, with the method exhibiting high precision across all tested C-rates, providing a robust solution for real-time monitoring and control [14]. Moreover, recent work has combined ECM with deep learning, such as using a fractional-order RC model optimized via hybrid fractional particle swarm optimization, paired with a vision transformer network, to achieve more accurate SOH estimations [15].

While traditional model-based methods are effective for estimating lithium battery SOH, they are hindered by high computational complexity and significant dependence on parameters, which restricts their broader application in practical scenarios.

Data-driven techniques to estimate SOH have grown in popularity in recent years thanks to advancements in machine learning and deep learning technology. Machine learning techniques generally focus on extracting features from historical data to build predictive models linked to the health of lithium batteries. Wang et al. introduced a method for predicting lithium battery SOH using differential thermal voltammetry (DTV) combined with Gaussian process regression (GPR). They applied a filtering method to smooth the DTV curve, extracted crucial features indicative of battery degradation, and used the GPR model for accurate SOH estimation [16]. Li et al. developed an adaptive boosting ensemble learning strategy combined with a particulate swarm optimization support vector machine (AdaBoost-PSO-SVM) for calculating SOC and SOH in lithium batteries. This approach enhances prediction accuracy by combining multiple weak learners [17]. Furthermore, Deng et al. have created a highly correlated SOH estimate model by employing a sparse Gaussian process regression approach with random partial charge data. By extracting the battery capacity increment series across different voltage segments, this method achieved average maximum absolute errors of just 2.88%, 2.52%, and 1.51% across three distinct battery types [18]. Zhang et al. proposed an SOH estimation method for Li-ion batteries using incremental capacity analysis and an improved Broad Learning System (BLS) network. They applied smoothing spline filtering to denoise voltage data and used particle swarm

optimization to enhance the BLS network, achieving high accuracy with low computational complexity [19].

Using deep learning approaches to describe complicated nonlinear systems and their high feature extraction capabilities, lithium battery SOH prediction has also benefited from their use. In order to increase SOH prediction accuracy across many datasets, Bao et al. introduced a hybrid deep neural network framework called CNN-VLSTM-DA [20]. Similarly, Liu et al. developed an LSTM network optimized with an enhanced Sparrow search algorithm for predicting battery remaining useful life (RUL) [21]. Van et al. utilized an LSTM network for SOH and internal resistance estimation, demonstrating its superior performance in extracting features from long-term data [22]. Tang et al. proposed a hybrid neural network to estimate SOH that incorporates a convolutional block attention module (CBAM) with an LSTM. This approach enhances CNN's feature extraction ability using an attention mechanism, allowing for highly accurate predictions under various operating conditions [23]. Zhang et al. suggested a technique for estimating SOH in lithium-ion batteries based on selected charging intervals, which included an incremental energy per SOC curve to examine aging features. The method employs a bidirectional LSTM-reduction network for estimation, demonstrating high accuracy and robustness [24]. Additionally, Fan et al. introduced an SOH estimation technique using a GRU-CNN hybrid model, which employs deep learning to capture shared information and temporal dependencies in the charging curve, leading to efficient SOH estimation [25]. Yang et al. proposed a novel SOC estimation method that utilizes a dual-stage attention mechanism within a deep learning framework. This approach incorporates domain-specific features—current, voltage, and temperature—within a gated recurrent unit (GRU)-based encoder-decoder network. By applying attention mechanisms in both the encoder and decoder stages, the model can adaptively extract relevant features and accurately estimate SOC despite noisy conditions. Validation tests on both proprietary and public datasets demonstrated the model's high accuracy, achieving a mean absolute error of less than 0.5% [26]. Li et al. introduced a hybrid deep learning model that combines temporal convolutional networks (TCNs) with gated recurrent units (GRUs) to leverage both parallel processing and sequential learning capabilities. By incorporating an attention mechanism, their model can dynamically prioritize important historical information, improving SOC estimation accuracy. Additionally, the use of a quantile regression loss function enables the model to generate interval estimates, providing more reliable predictions. Testing on lithium iron phosphate, lithium cobalt oxide, and ternary lithium batteries yielded mean absolute errors and root mean square errors below 1.45 and 1.98, 1.12 and 1.25, and 0.61 and 0.75, respectively [27].

Hybrid models take advantage of the strengths of various algorithms to improve the accuracy and robustness of battery SOH prediction. Jiang et al. developed a cyclic aging prediction method using a multi-kernel relevance vector machine combined with a PSO algorithm. By optimizing kernel parameters, this approach accurately forecasts the degradation trajectories of different battery types [28]. Li et al. introduced a time series forecasting method that integrates Bi-GRU with SSA, originally applied in oilfield production forecasting. This method can also be adapted for battery SOH prediction, where optimizing model hyperparameters further enhances prediction accuracy [29]. Additionally, Wu et al. proposed a data-driven transfer learning model that achieves high-precision SOH prediction while using only 30% of the target battery data by combining SVR with the Transfer Stacking (TS) method [30].

Feature engineering and transfer learning techniques are utilized to extract essential battery features, enhancing model performance. Wang et al. introduced an SOH estimation method based on feature engineering, which adapts laboratory data to real-world operating conditions by downscaling. This method demonstrates strong predictive performance even when dealing with incomplete datasets [31]. Xu et al. developed an improved CNN-LSTM model, where the neural network input is optimized through a feature selection process, leading to increased accuracy and computational efficiency in SOH prediction [32].

Data preprocessing techniques are also an important area of focus. Wen et al. proposed an SOH prediction model based on incremental capacity analysis combined with BP neural networks, achieving high-precision SOH prediction by analyzing the relationship between IC curves and temperature characteristics [33]. Chen et al. introduced a method leveraging temperature prediction and GRU neural networks, which achieves high-accuracy SOH prediction through multi-dimensional health feature extraction [34]. In order to facilitate effective and quick SOH prediction, Lin et al. created a rapid SOH estimate approach based on constant current charging time (CCCT) and using random forest regression [35]. Zhang et al. suggested a battery SOH estimate technique based on gradient current, dual correlation analysis, and a GRU model optimized with a sparrow search algorithm. This approach selects SOH-related features and achieves high-precision SOH estimation [36].

In lithium battery SOH prediction, while data-driven methods offer high accuracy and flexibility, they also present notable drawbacks. These approaches heavily rely on the quality and quantity of training data, leading to significant performance degradation when the data are incomplete or noisy. Additionally, the complexity of these models demands substantial computing resources, making both time and economic costs relatively high. Consequently, future research should focus on addressing these limitations to enhance the usability and robustness of these models.

Given the strengths and limitations of current data-driven methods, we propose a novel approach that combines Kolmogorov–Arnold Networks (KAN) with the Long Short-Term Memory (LSTM) algorithm for lithium battery State of Health (SOH) estimation. The KAN component is utilized for its capability to effectively map complex, nonlinear relationships, while the LSTM algorithm excels at capturing long-term dependencies in sequential data. By integrating these two methods, the approach enhances feature extraction and temporal pattern recognition, resulting in a significant improvement in SOH estimation accuracy. The main contributions of this paper are summarized as follows.

- (1) During the constant current and constant-voltage charging stages, data were analyzed to derive a wide range of comprehensive information. Initially, voltage, current, and temperature data were measured during these charging stages to extract relevant features. By plotting these features against the battery SOH, those with a strong correlation to SOH were identified. These selected features were then combined with the battery's temperature characteristics to form a complete multi-feature sequence.
- (2) An efficient KAN-LSTM deep learning model is constructed. In this study, Kolmogorov–Arnold Networks (KAN) are used to extract key trends from the sequence, successfully reducing the original multi-feature sequence to localized abstract characteristics and minimizing the computational load on the following model. Following the KAN, a Long Short-Term Memory (LSTM) network is employed to collect long-term interactions, enabling the tracking of the battery SOH aging process. Additionally, the inclusion of a Dropout layer enhances the model's stability. As a result, the KAN-LSTM model demonstrates outstanding performance in SOH estimation, excelling in terms of accuracy, speed, and robustness.
- (3) This paper presents a comprehensive and detailed validation of the SOH estimation method, focusing on four main aspects: First, experiments were conducted using four different charge rate battery aging datasets (own data) to estimate battery SOH. Second, the effect of temperature features on SOH estimation results was examined, exploring the accuracy variations under different temperature conditions. Third, the suggested KAN-LSTM model was systematically compared against the LSTM, CNN+LSTM, BiLSTM, and CNN-BiLSTM models to assess performance differences in SOH estimation. Finally, further tests were performed on the NASA battery dataset to confirm the efficiency of the technique. The experimental findings show the fact that despite the nonlinear deterioration process of battery SOH, the technique has a significant SOH estimate capacity. Specifically, across all four datasets, the mean absolute error (MAE) remained within 0.6%, the root mean square error (RMSE) was below 0.8%, and the average coefficient of determination ( $R^2$ ) exceeded 97%. In

summary, through comprehensive experiments using both own data and the NASA dataset, this work establishes a high-accuracy SOH estimation model and further validates its effectiveness through comparative analysis.

The remainder of this paper is organized as follows: Sections 2 and 3 introduce the experimental dataset and its preprocessing methods, along with a detailed analysis of the features. Section 4 presents the proposed KAN-LSTM model and explains its advantages. Section 5 describes the experimental procedures, including model evaluation metrics, SOH estimation results, multi-model comparisons, result analysis, and the impact of temperature characteristics. Additionally, cross-dataset and cross-battery prediction experiments are discussed to further validate the generality of the proposed method. Finally, Section 6 concludes the paper.

## 2. Experimental Dataset and Preprocessing

In this study, four cylindrical lithium batteries with identical specifications were subjected to charging and discharging cycle aging experiments at indoor ambient temperature using professional experimental equipment. The experimental setup is depicted in Figure 1. The system comprises a host computer and a battery tester, forming a comprehensive battery charge and discharge cycle test system. This setup can perform various charging and discharging modes, including constant current charging, constant-voltage charging, and constant discharge.

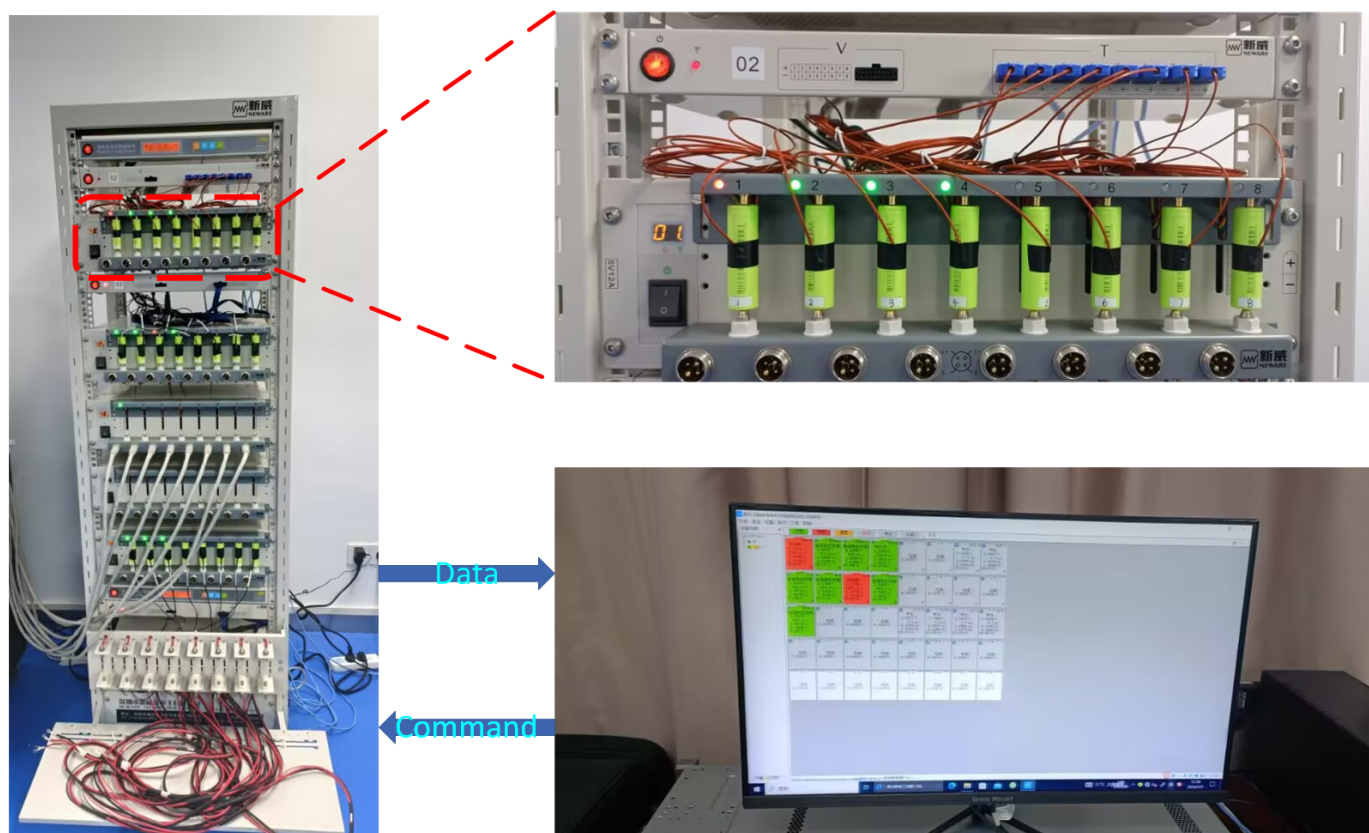


**Figure 1.** Experimental equipment diagram.

Each battery has a standard capacity of 2.5 Ah and operates according to a specific charge and discharge cycle, which is divided into two main phases: charging and depletion phases. The charging process typically involves two stages: constant current charging followed by constant-voltage charging.

Throughout the constant current charging phase, each battery is charged at a constant current until the voltage reaches 4.2 V. Then, the battery enters the constant-voltage phase,

maintaining the voltage at 4.2 V until the charging current drops below 48 mA, indicating the charging process is complete.

Once charging is complete, the battery is given a break for 5 min to stabilize before proceeding to the discharge phase. During the discharge phase, the battery is drained at a current determined by its unique discharge characteristics till the voltage drops to 3 V, completing the whole charge–discharge cycle.

### 3. Feature Analysis

The charging cycle in this study comprises the following steps: Initially, constant current charging is performed, followed by a transition to constant-voltage charging once a specific voltage is reached, and finally, constant current discharge is conducted. The feature extraction in this study primarily focuses on the charging phase of the cycle, as illustrated in Figure 2.

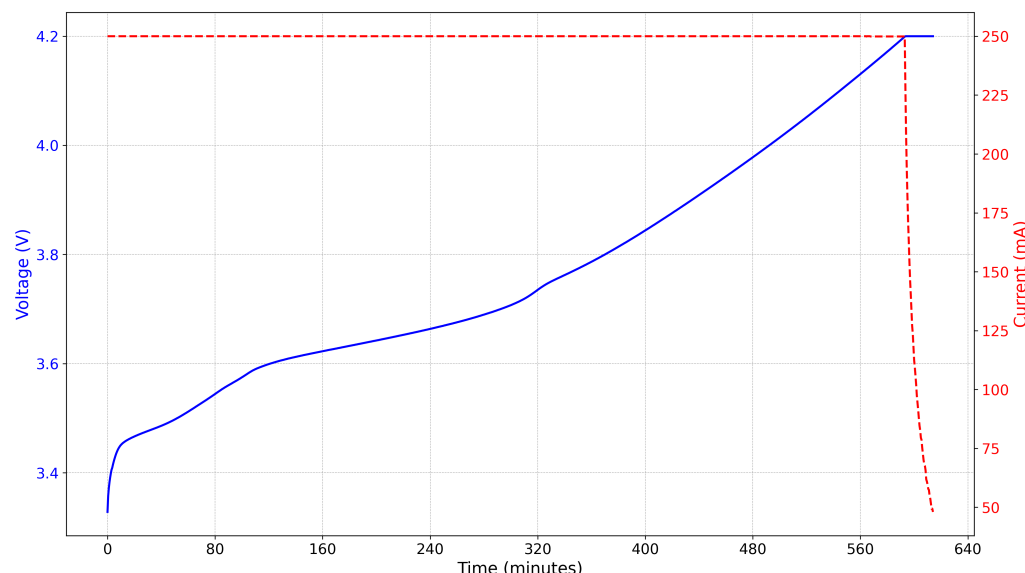


**Figure 2.** Voltage and current curves while charging.

During the constant current charging phase, the focus is primarily on voltage variation since the charging current remains constant. The voltage behavior during constant current charging across different battery cycles is depicted in Figure 3. All voltage curves exhibit a rapid initial increase, followed by a gradual deceleration in the rate of growth.

Because constant current charging is employed, the charge amount may be determined using Equation (1).

$$Q = I \cdot t \quad (1)$$

$Q$  is the amount of charge given to the battery,  $I$  is the continuous charging current, and  $t$  signifies the charging period.

As the number of battery charging cycles increases, the time required for the voltage curve to peak decreases. This indicates that the amount of energy required to charge the battery from 3 V to 4.2 V decreases with each subsequent use, reflecting a gradual degradation in battery performance.

Therefore, one of the model's input parameters in this study is the constant current charging time. Figure 4a illustrates the variation of constant current charging time with the number of battery charging cycles. The charging time exhibits a decreasing trend as the number of charging cycles increases.

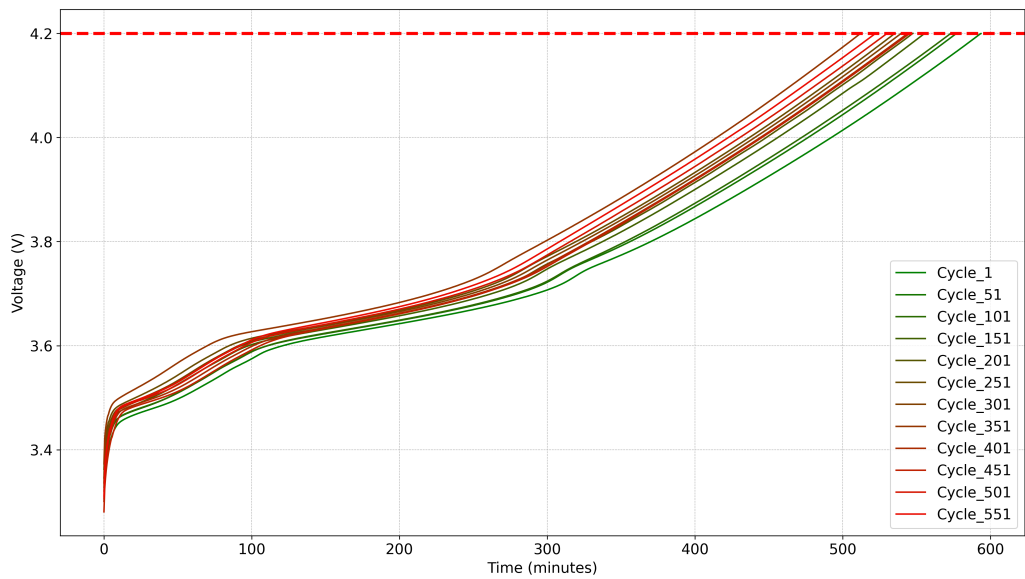


**Figure 3.** Variation of voltage curve with charging times in constant current charging state.

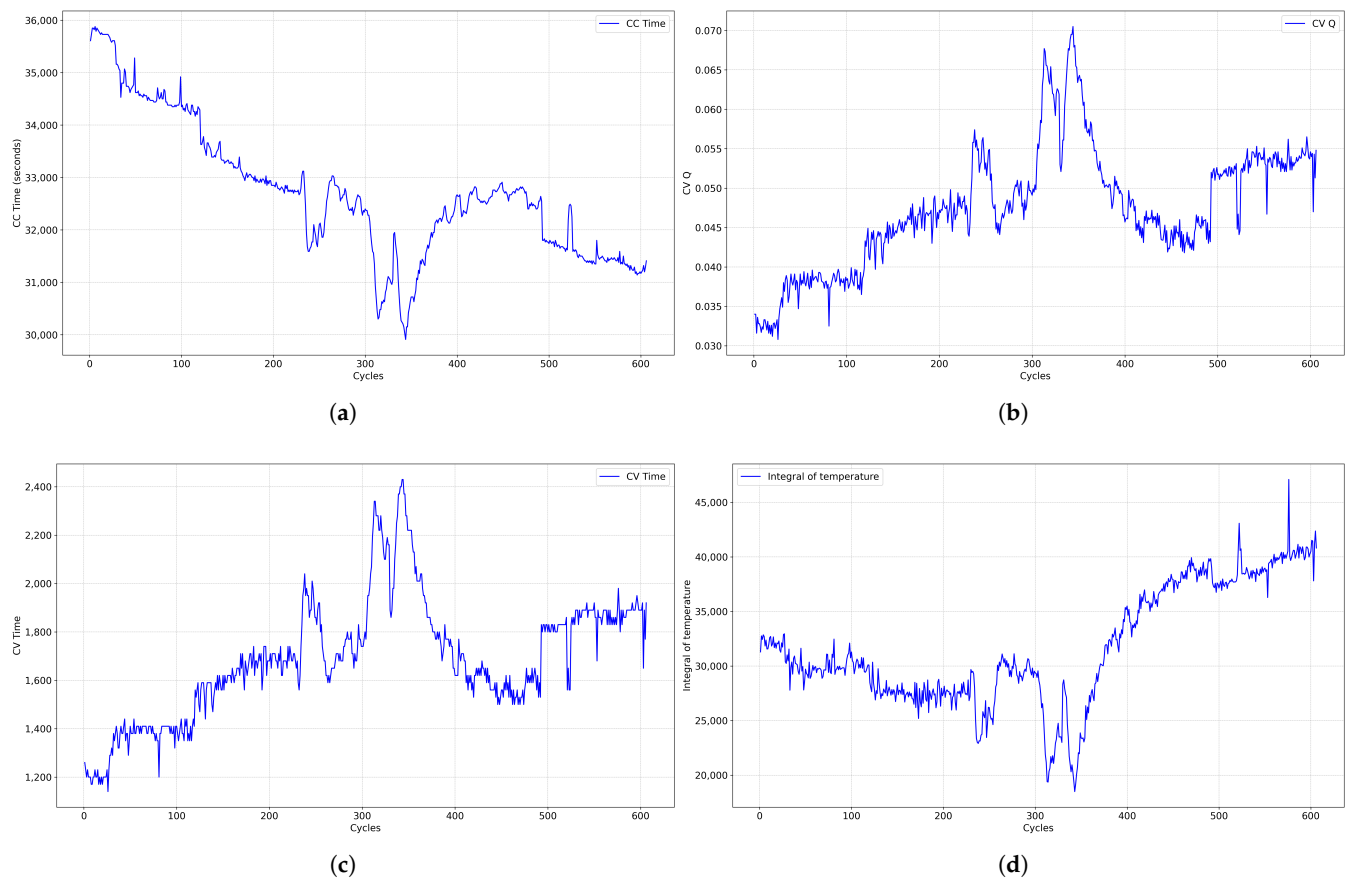


**Figure 4.** Characteristic pattern. (a) Constant current charging time; (b) The amount of electricity charged at constant voltage; (c) Constant-voltage charging time; (d) Integral of temperature.

In the constant-voltage charging stage, where the charging voltage remains constant, the focus is primarily on the current variation. The constant-voltage charging current across different battery charging cycles is depicted in Figure 5. All current curves exhibit a rapid initial decrease, followed by a gradual deceleration in the rate of decline.

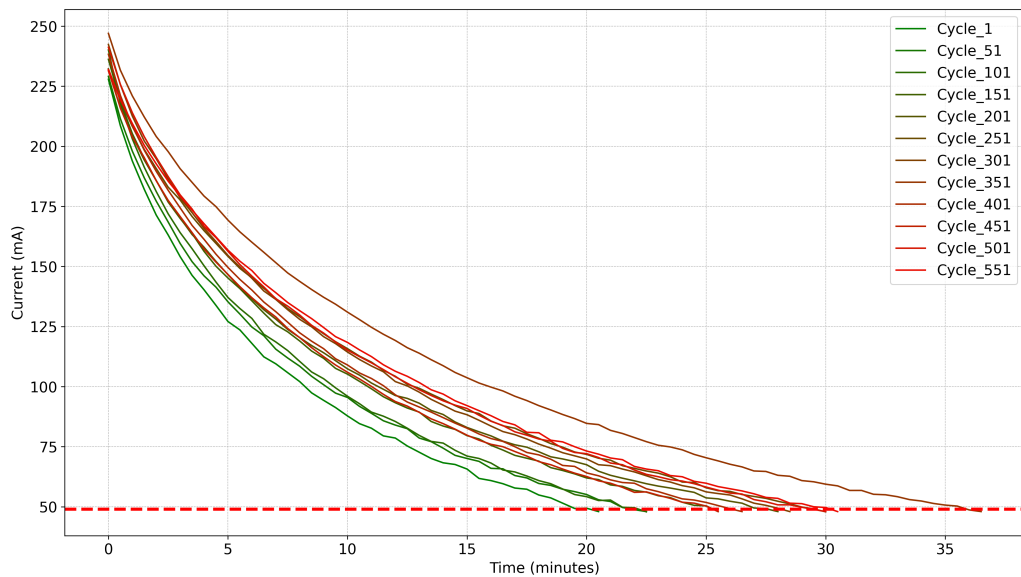


**Figure 5.** Curve of current versus charging times in constant-voltage charging state.

In this scenario, the current varies with time, and the charge quantity can be calculated using Equation (2).

$$Q = \int I(t) dt \quad (2)$$

where  $Q$  represents the amount of charge delivered to the battery, and  $I(t)$  is the current at time  $t$ .

The numerical value corresponds to the area under the curve in the graph. As the number of battery charging cycles rises, so does the quantity of charge, as shown by the corresponding area.

During the constant-voltage charging stage, this study used both the constant-voltage charging time and the constant-voltage charging amount. Figure 4b,c show how these two features vary with the amount of battery charging cycles. Both parameters show an increasing tendency as the number of battery charging cycles rises. The qualities described above have a significant association with lithium battery SOH. Figure 6 shows a comprehensive analysis based on data from a single battery, as detailed in Figure 6a–c. According to relevant literature, features with a high correlation to the target should be selected for machine learning [37–39].

Related papers have indicated that the SOH of lithium batteries is significantly influenced by environmental temperature. Therefore, this study also incorporated the integral temperature obtained during the constant-voltage charging stage as a temperature-related feature. Figure 6d shows the graph of the integral temperature across the battery charging cycles during the constant-voltage charging phase. Although the linear correlation between battery SOH and temperature integration is not very apparent, as observed in Figure 6d, further analysis reveals a certain nonlinear relationship between them. This suggests that temperature may impact battery SOH not only through direct linear effects but also via more complex mechanisms affecting the aging process. While temperature integration alone might not directly linearly predict SOH, its combined analysis with other features can offer a more comprehensive assessment of battery health.

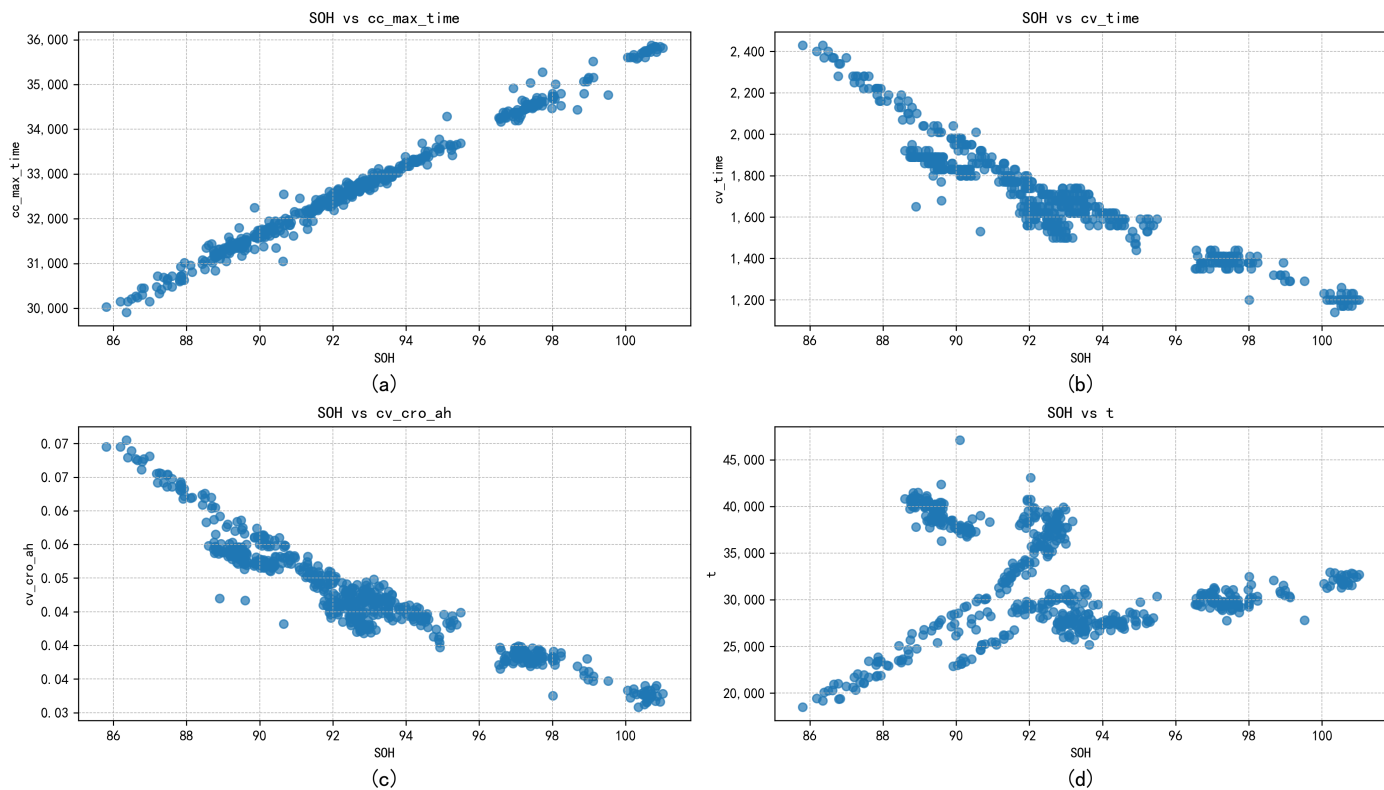


**Figure 6.** Relational graph.

#### 4. SOH Predict Strategy

In this study, a hybrid model combining the Kolmogorov–Arnold Network (KAN) and Long Short-Term Memory Network (LSTM) is proposed for battery lifetime prediction. The KAN network employs learnable activation functions on the network's edges to capture complex nonlinear patterns in battery data, while the LSTM is used to handle time series data, which captures the change in battery states over time.

##### 4.1. Kolmogorov–Arnold Network (KAN)

Compared to the traditional Multilayer Perceptron (MLP), the KAN network incorporates an adjustable activation function (typically a spline function) that replaces the fixed weights and activation functions in traditional neural networks. This allows KAN to adapt to the nonlinear relationships within the data. This structure enables KAN to excel in feature extraction and to be dynamically adjusted during model training, which enhances its ability to capture the complex patterns inherent in the data. These properties make KAN networks particularly suitable for capturing the intricate nonlinear patterns present in battery data, which is why they are employed in this study.

The Kolmogorov–Arnold representation theorem, which states that any continuous function can be written as a composition of a collection of unary functions, is the foundation of KAN theory.

For any continuous function  $f$ , there exists a set of unary functions  $\phi_{ij}$  and  $\psi_i$  such that

$$f(x_1, x_2, \dots, x_n) = \sum_{i=1}^{2n+1} \psi_i \left( \sum_{j=1}^n \phi_{ij}(x_j) \right) \quad (3)$$

The unary functions  $\phi_i$  and  $\psi$  are represented and learned by B-splines, which are basis functions used to construct other functions. The core concept of B-splines is to represent a complex curve as a series of simple polynomial segments, each connected by control points.

The B-spline basis function  $B_{i,k}(t)$  can be defined recursively as follows:

$$B_{i,0}(t) = \begin{cases} 1, & t_i \leq t < t_{i+1}, \\ 0, & \text{otherwise.} \end{cases} \quad (4)$$

$$B_{i,k}(t) = \frac{t - t_i}{t_{i+k} - t_i} B_{i,k-1}(t) + \frac{t_{i+k+1} - t}{t_{i+k+1} - t_{i+1}} B_{i+1,k-1}(t) \quad (5)$$

here,  $t_i$  is the node in the node sequence, which defines the segment position and parameter range of the curve.

Thus, each unary function can be expressed using B-splines as follows:

$$\phi_{ij}(x_j) = \sum_{m=0}^k c_{ijm} B_{m,k}(x_j) \quad (6)$$

where  $c_{ijm}$  represents the weight of the control points, and  $B_{m,k}(x_j)$  is the corresponding B-spline basis function. By learning the weights of these control points, KAN can dynamically adjust the shape of each activation function.

In the KAN layer, the input  $X$  is processed through a set of learnable B-spline activation functions  $\phi_{ij}$  and  $\psi_i$ , which are then summed at the nodes. The output of the KAN layer is stated as follows:

$$y_i = \psi_i \left( \sum_{j=1}^n \phi_{ij}(x_j) \right) \quad (7)$$

Figure 7 illustrates the framework of the KAN network.

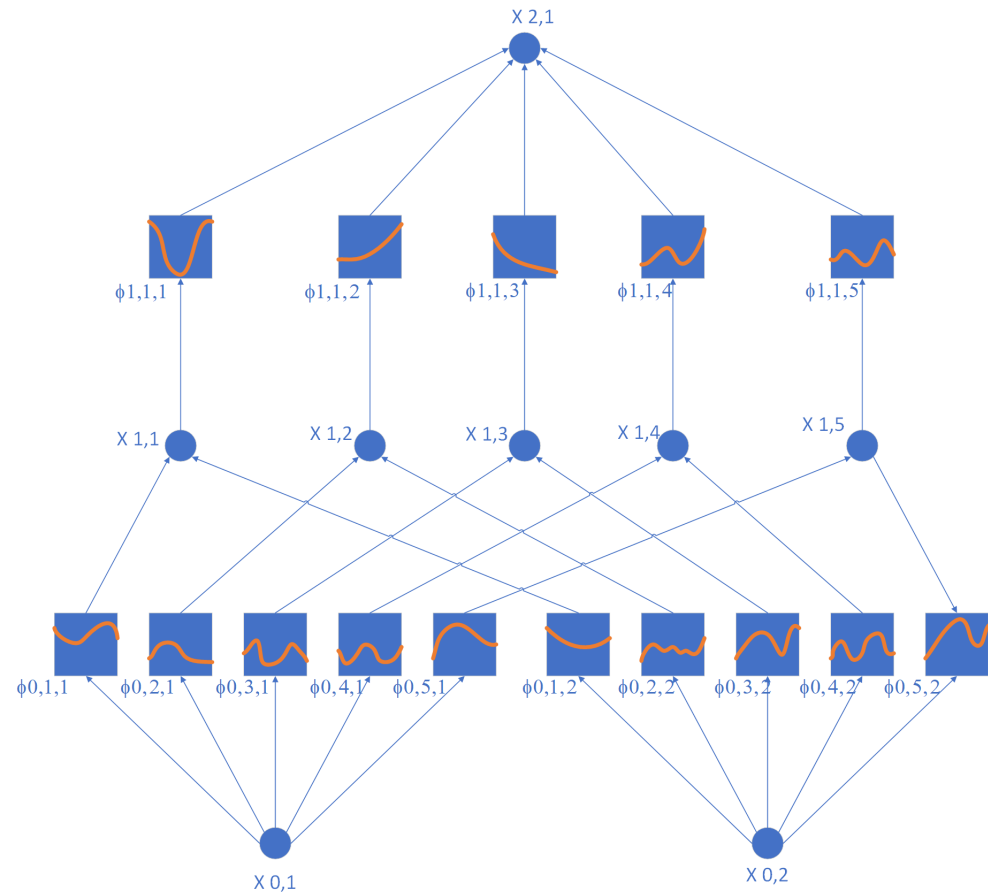


**Figure 7.** KAN model structure.

#### 4.2. Long Short-Term Memory Networks (LSTM)

LSTMs are commonly employed in sequence-to-sequence problems, including language translation, audio recognition, machine translation, along with time series prediction. LSTM is a form of recurrent neural network (RNN) that can efficiently capture long-term relationships in time series data. In this study, LSTM is used to interpret time series data and forecast the life of lithium batteries. The input sequence contains characteristics taken from the battery data that have gone through the KAN layer output, and the output is the battery's state of health.

The LSTM unit operates by controlling the flow of information and updating the state at each time step through a set of gating mechanisms.

The forget gate determines how much past state information the current cell should delete. It is expressed using the following formula:

$$f_t = \sigma(W_f \cdot [h_{t-1}, x_t] + b_f) \quad (8)$$

The forget gate's output is denoted by  $f_t$  in this case. The input at the current time step is  $x_t$ . The weight matrix and bias vector to be learned are  $W_f$  and  $b_f$ . The hidden state of the previous LSTM cell is  $h_{t-1}$ .

The input gate establishes the amount of fresh data that must be entered into the current cell. It may be expressed using the following formula:

$$i_t = \sigma(W_i \cdot [h_{t-1}, x_t] + b_i) \quad (9)$$

In this case, the input gate's output is denoted by  $i_t$ , and the weight matrix and bias vector that needs to be learned are  $W_i$  and  $b_i$ .

Candidate memory unit: Generates new candidate memory content. It may be expressed using the following formula:

$$\tilde{C}_t = \tanh(W_C \cdot [h_{t-1}, x_t] + b_C) \quad (10)$$

The weight matrix and bias vector that need to be learned are  $W_C$  and  $b_C$ , whereas the new candidate memory cell is denoted as  $\tilde{C}_t$ .

Updating the memory cell's state involves combining the forget and input gates. The following formula gives its expression:

$$C_t = f_t \cdot C_{t-1} + i_t \cdot \tilde{C}_t \quad (11)$$

here,  $C_t$  is the updated memory cell state.

The current cell's output is determined by the output gate. The following formula gives its expression:

$$\begin{aligned} o_t &= \sigma(W_o \cdot [h_{t-1}, x_t] + b_o) \\ h_t &= o_t \cdot \tanh(C_t) \end{aligned} \quad (12)$$

In this case, the hidden state at the current time step is denoted by  $h_t$ , while the output of the output gate is represented by  $o_t$ .

Figure 8 depicts the architecture of a Long Short-Term Memory network (LSTM).

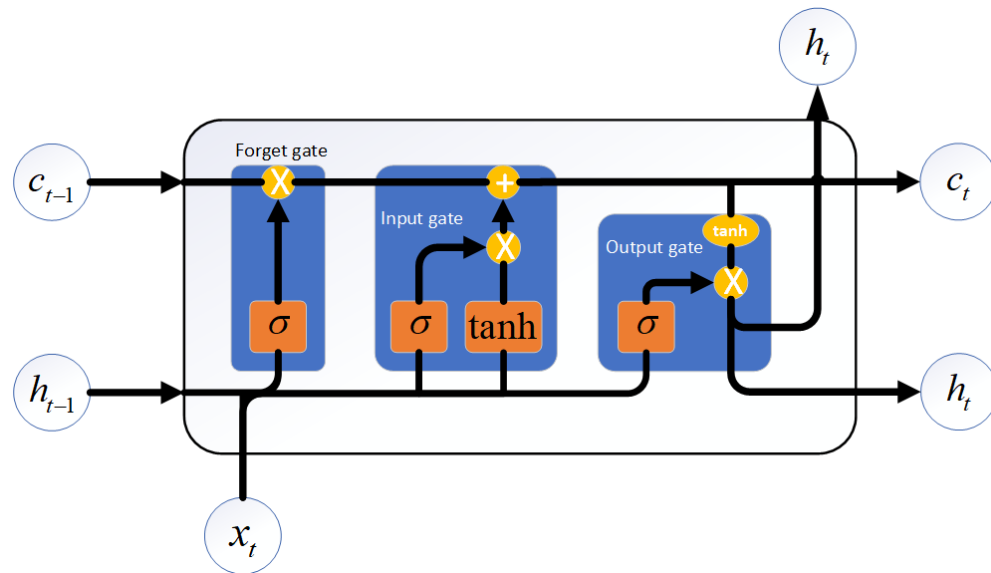


**Figure 8.** LSTM Model Structure.

## 5. Experimental Procedure

The experimental steps of this study are illustrated in Figure 9. The characteristics of lithium-ion batteries that we retrieved are detailed in Section 3. These features include the integral of temperature during the constant-voltage charging phase, constant current charging time, constant-voltage charging quantity, and constant-voltage charging time. To create a complete dataset, these attributes were combined with the corresponding SOH values. The dataset was split 1:1 into a training and test set in order to maintain a balanced distribution and ensure the model's ability to generalize. The first 50% of the data periods were utilized for the training data set, while the remaining 50% were assigned to the test data set.

The training data are fed into the KAN-LSTM model, which integrates KAN and LSTM. The number of units in the KAN layer and the number of hidden units in the LSTM layer are determined by the dataset used in this model. For instance, in a typical configuration, the KAN layer may be set to 16 units to enhance the input features, while the LSTM layer could be configured with 64 hidden units to capture temporal dependencies in the data. To prevent overfitting, a Dropout layer with a drop rate of 0.1 is added after the LSTM output. Finally, the output of the LSTM is mapped to the final SOH prediction value through a fully connected layer.

During training, the Adam optimizer is used to optimize the model parameters. The model is trained for 250 epochs, and performance evaluation is based on  $R^2$  scores. The best-performing model is saved. The experimental results are then analyzed by loading the best-performing model and making predictions on the test set.

Table 1 displays each battery's charging as well as discharge parameters.

**Table 1.** Battery charging and discharging parameters.

Battery Number	Charging/Discharging	Description
1	0.1 C/0.5 C	charge at 0.1 C, discharge at 0.5 C.
2	0.1 C/ 1 C	charge at 0.1 C, discharge at 1 C.
3	0.2 C/0.5 C	charge at 0.2 C, discharge at 0.5 C.
4	0.2 C/ 1 C	charge at 0.2 C, discharge at 1 C.

This experiment began on 16 August 2023, and the charging and discharging cycle tests were conducted continuously. The data for this study encompasses all information collected between 16 August 2023 and 6 July 2024. The dataset includes voltage, current,

and temperature information for each charge and discharge cycle, which were used to calculate the charging and discharging capacities for each cycle.

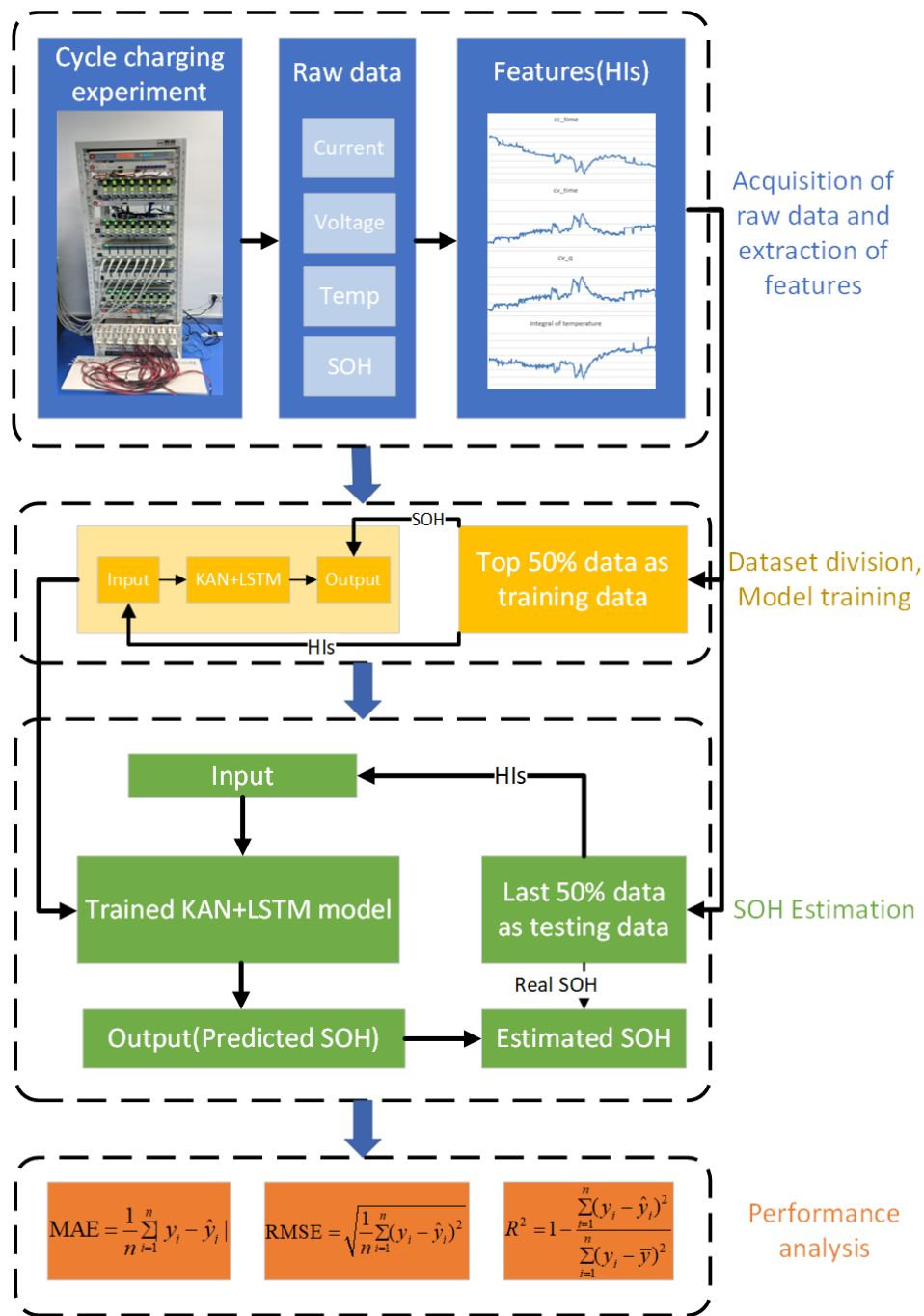


**Figure 9.** Flow chart of the experimental steps.

In this study, the health status of the battery was defined as the ratio of the current capacity to the calibrated capacity.

$$SOH = \frac{Q_{\text{max capacity}}}{Q_{\text{rated capacity}}} \times 100\% \quad (13)$$

where  $Q_{\text{max capacity}}$  represents the current maximum discharge capacity of the battery, determined by integrating the discharge current over a complete discharge cycle, and  $Q_{\text{rated capacity}}$  is the calibrated nominal capacity of the battery, which is 2.5 Ah.

The graph of the SOH of the four batteries as a function of the number of charging cycles is shown in Figure 10. Each subfigure illustrates the process where the battery starts at nearly 100% SOH and gradually decreases during the charge and discharge cycles, exhibiting varying degrees of fluctuation and a downward trend. The first battery experienced a sharp decline in the middle of the cycle, followed by a slight recovery and then a slow decline. The second battery exhibited several significant drops and recoveries, ultimately reducing its SOH to around 82%. The SOH of the third battery decreased from 100% to below 75%, with the overall decline being relatively gradual. In contrast, the fourth battery showed a consistent downward trend over multiple cycles, eventually falling below 75%. The large fluctuations in these curves may be attributed to seasonal factors, where certain conditions cause the battery to endure significant load or stress, leading to capacity decline and subsequent recovery.

The aging parameters are shown in Table 2.

**Table 2.** Battery charge and discharge data and SOH data.

Battery	Cycles	Initial SOH (%)	Final SOH (%)
1	608	100.528	88.600
2	677	98.400	82.440
3	998	99.436	75.492
5	1136	99.616	61.216

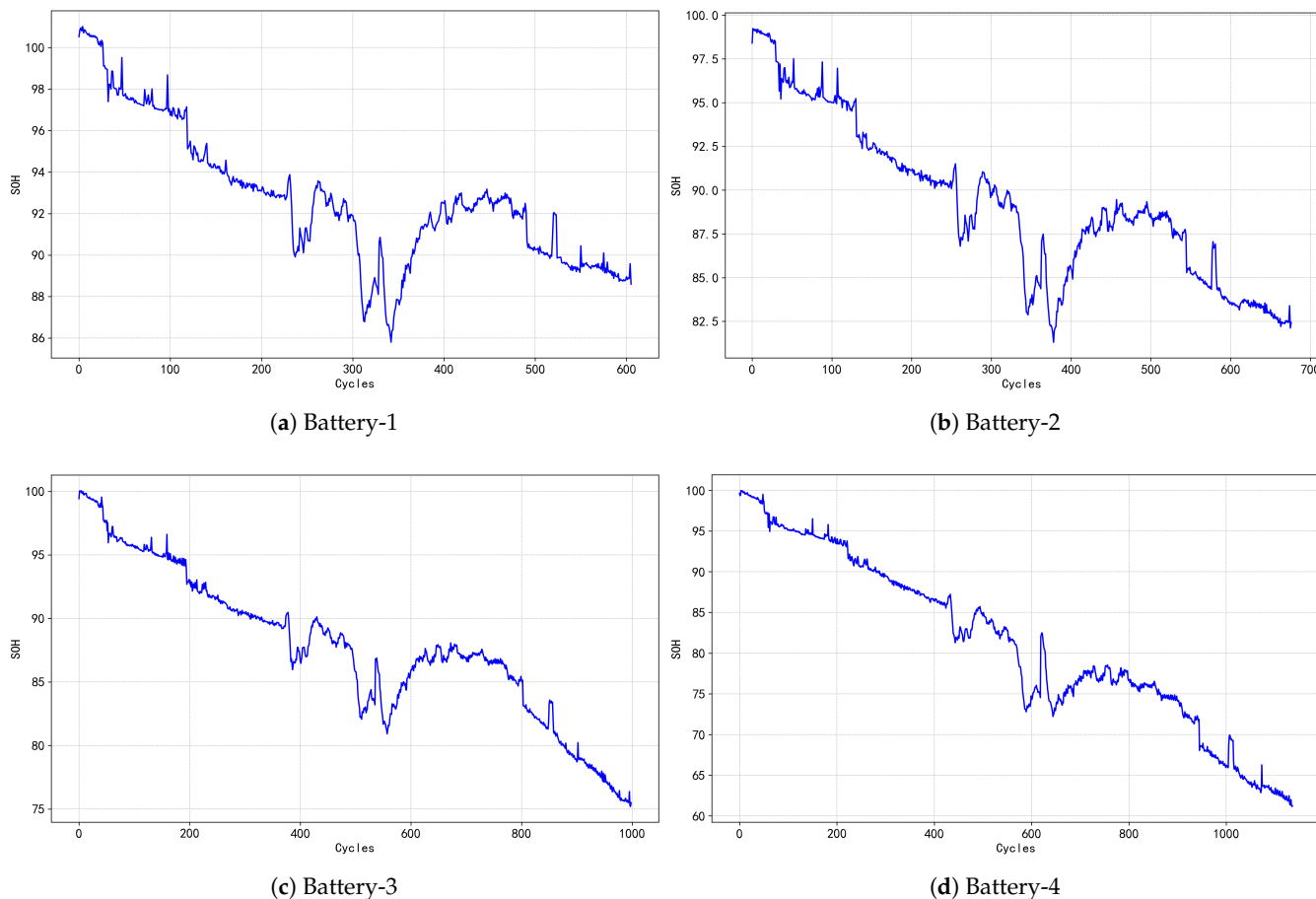


**Figure 10.** The curve of SOH versus the number of charging times.

Based on the above description, the model's input features include constant current charging time, constant-voltage charging time, constant-voltage charging quantity, and the integral of temperature during the constant-voltage charging phase, all of which have

a direct impact on battery life. After data preprocessing and feature extraction, the final input features to the model are the standardized versions of these variables.

### 5.1. Model Evaluation Criteria

The core metrics commonly used in the evaluation of statistical models include mean absolute error (MAE), root mean square error (RMSE), and the coefficient of determination ( $R^2$ ). These metrics allow us to quantify the accuracy and effectiveness of model predictions from different perspectives. This study used MAE, RMSE, and  $R^2$  to measure the model's performance.

MAE is derived by averaging the absolute differences between anticipated and actual values, indicating the predicted values' average degree of departure from the actual values.

The RMSE is determined by first squaring the differences between anticipated and actual values, then averaging the squared differences, and lastly, calculating the square root of the result. Since RMSE magnifies the impact of larger errors, it is more suitable for application scenarios that are particularly sensitive to large errors.

$R^2$  measures the correlation between anticipated and actual values, indicating the model's ability to explain variability in the data. The model's prediction performance and fit improve as the  $R^2$  value approaches 1.

The above parameters are calculated as follows:

$$\text{MAE} = \frac{1}{n} \sum_{i=1}^n |y_i - \hat{y}_i| \quad (14)$$

$$\text{RMSE} = \sqrt{\frac{1}{n} \sum_{i=1}^n (y_i - \hat{y}_i)^2} \quad (15)$$

$$R^2 = 1 - \frac{\sum_{i=1}^n (y_i - \hat{y}_i)^2}{\sum_{i=1}^n (y_i - \bar{y})^2} \quad (16)$$

here,  $y_i$  represents the actual battery SOH value,  $\hat{y}_i$  is the SOH value predicted by the model based on the input features, and  $\bar{y}$  is the arithmetic mean of the actual observations  $y_i$ .

### 5.2. SOH Estimation Results

In the experiment, we used the KAN-LSTM model mentioned above to predict the battery health state (SOH). The result is shown in Figure 11.

To test the suggested method's estimated performance, we conducted experiments utilizing the three evaluation metrics described earlier: MAE, RMSE, and  $R^2$ . Table 3 contains comprehensive information.

The MAE for all test data is within 0.6%, while the RMSE is within 0.8% across charging rates. This shows that the suggested approach can properly estimate the SOH of the battery.

**Table 3.** Performance of KAN-LSTM in estimating SOH at four charging rates.

Battery	MAE (%)	RMSE (%)	$R^2$ (%)
1	0.2043	0.2896	97.21
2	0.2561	0.3667	97.42
3	0.2756	0.4256	97.34
4	0.5705	0.7645	98.04

### 5.3. Comparing Multiple Models

To demonstrate the superiority of the suggested KAN-LSTM model, we compared it to others. The experiment utilized data from different charging schemes to compare and analyze the estimation results of each model under varying conditions, as shown in Figure 12. The results, including the calculation of MAE, RMSE,  $R^2$ , and other metrics, are presented in Tables 4–7.

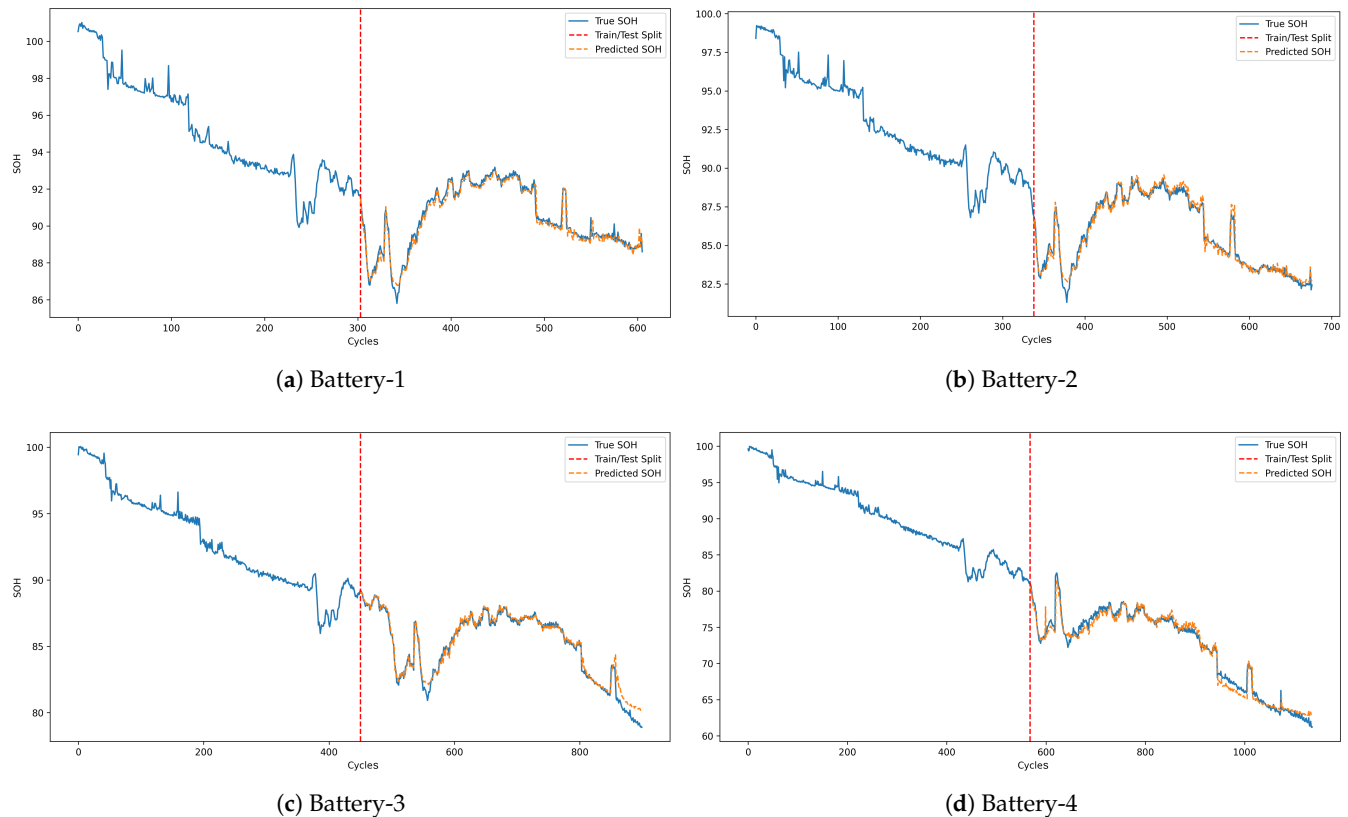


**Figure 11.** Graph of the prediction results of the KAN-LSTM model.

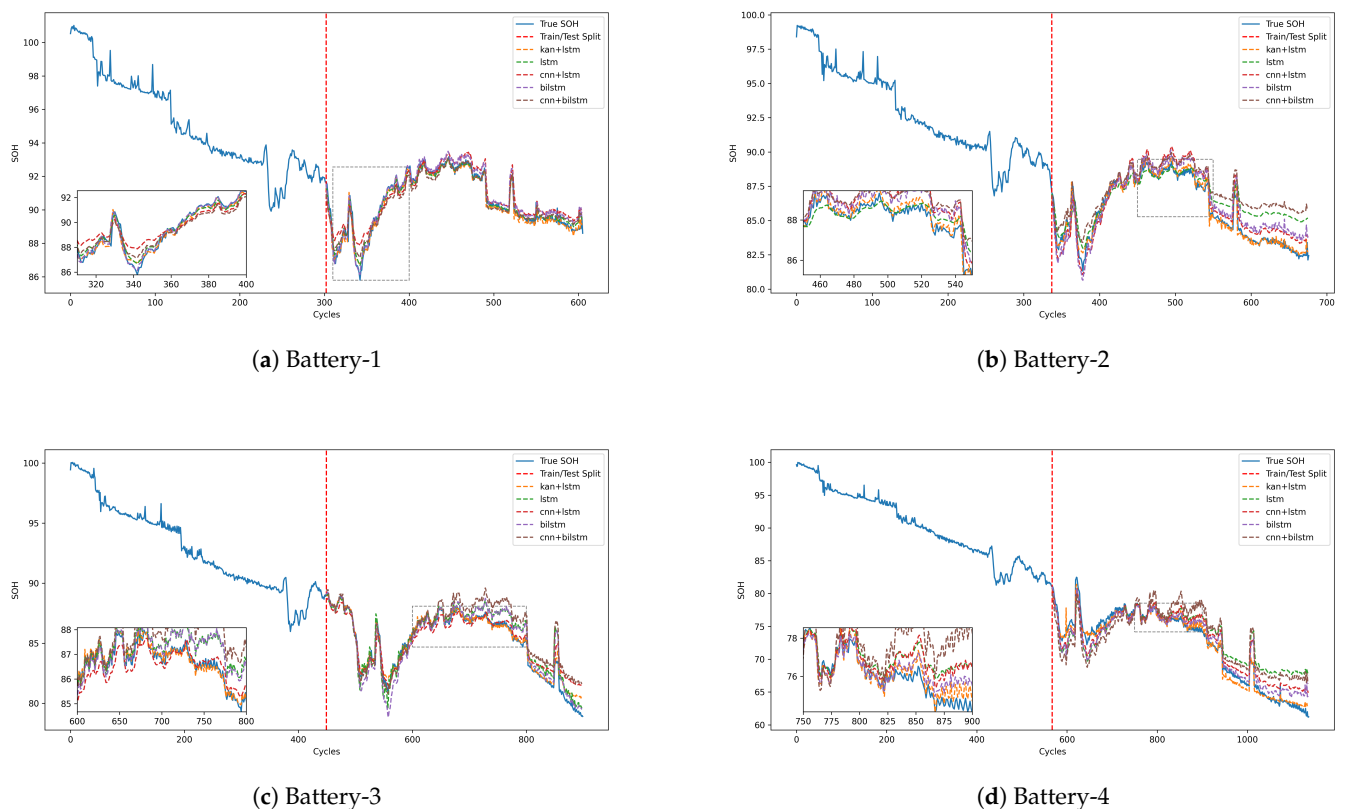


**Figure 12.** Comparison of the prediction results of each model.

**Table 4.** Comparison of Different Models Based on MAE, RMSE, and  $R^2$  (Battery 1).

Model	MAE (%)	RMSE (%)	$R^2$ (%)
KAN-LSTM	0.2043	0.2896	97.21
LSTM	0.2368	0.3368	96.23
CNN-LSTM	0.5045	0.6249	87.01
BILSTM	0.2810	0.3538	95.84
CNN-BILSTM	0.3480	0.4475	93.34

**Table 5.** Comparison of Different Models Based on MAE, RMSE, and  $R^2$  (Battery 2).

Model	MAE (%)	RMSE (%)	$R^2$ (%)
KAN-LSTM	0.2561	0.3667	97.42
LSTM	1.0380	1.3438	65.44
CNN-LSTM	0.7740	0.8874	84.93
BILSTM	0.7913	0.9046	84.34
CNN-BILSTM	1.3979	1.7047	44.39

**Table 6.** Comparison of Different Models Based on MAE, RMSE, and  $R^2$  (Battery 3).

Model	MAE (%)	RMSE (%)	$R^2$ (%)
KAN-LSTM	0.2756	0.4256	97.34
LSTM	0.5964	0.7803	91.05
CNN-LSTM	0.6502	0.8912	88.33
BILSTM	0.6666	0.8670	88.95
CNN-BILSTM	1.0350	1.3258	74.17

**Table 7.** Comparison of Different Models Based on MAE, RMSE, and  $R^2$  (Battery 4).

Model	MAE (%)	RMSE (%)	$R^2$ (%)
KAN-LSTM	0.5705	0.7645	98.04
LSTM	2.2594	2.8164	73.43
CNN-LSTM	1.4647	1.7687	89.52
BILSTM	1.1524	1.4609	92.85
CNN-BILSTM	2.6722	2.9779	70.29

The results indicate that the KAN-LSTM model excels in many aspects and outperforms several traditional models. Particularly under multiple charging rates, the KAN-LSTM model demonstrates higher prediction accuracy and smaller errors, showcasing its strong feature extraction capabilities and ability to process temporal information. The experimental findings show that the KAN-LSTM model can capture the complicated non-linear correlations in battery life decline, demonstrating its usefulness and dependability in health monitoring.

#### 5.4. Analysis of Results

The experimental results indicate that the standalone LSTM model is less accurate in its predictions compared to the KAN+LSTM model. When the KAN layer is combined with the LSTM layer, the prediction results show a marked improvement, with the KAN+LSTM model outperforming other combined models. This suggests that the features extracted by the KAN layer enhance the correlation between input features, effectively integrating key information and improving the completeness and accuracy of feature representation. Additionally, the KAN layer performs an initial compression and selection of features, reducing the computational burden on the subsequent LSTM layer and increasing the model's efficiency.

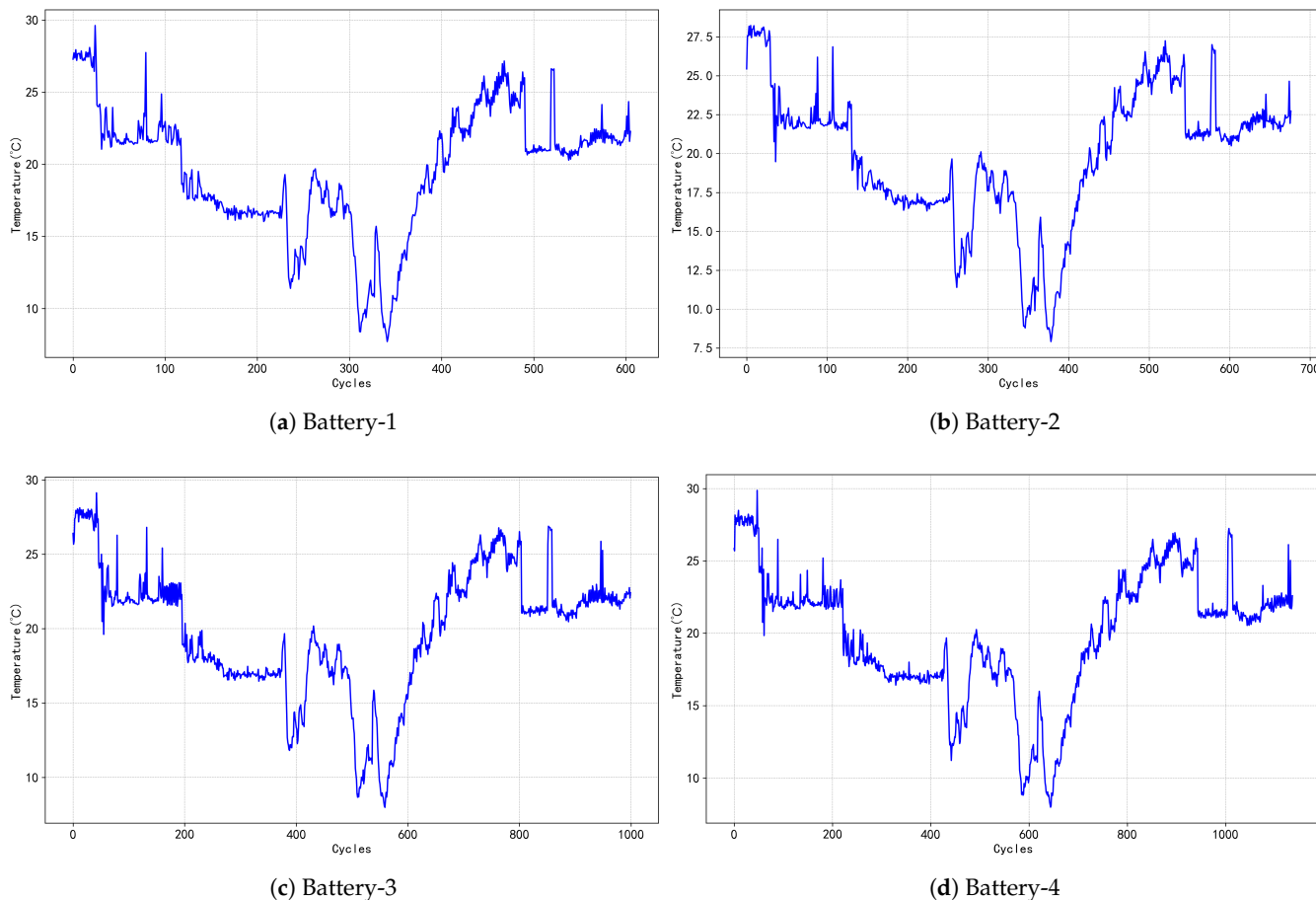
Furthermore, the LSTM layer excels in capturing temporal correlations, enabling the model to accurately recognize and predict SOH trends. In the KAN+LSTM model, the LSTM layer effectively utilizes the high-quality features extracted by the KAN layer, capturing the complex dynamic changes in the battery health state more accurately. The inclusion of a Dropout layer also enhances the model's stability and generalization ability, mitigating overfitting and further improving the model's adaptability across different datasets and charging conditions.

In summary, the KAN+LSTM model, with its advantages in feature extraction and time series processing, significantly improves the accuracy and stability of SOH estimation, demonstrating its practicality and superiority in monitoring complex battery health states.

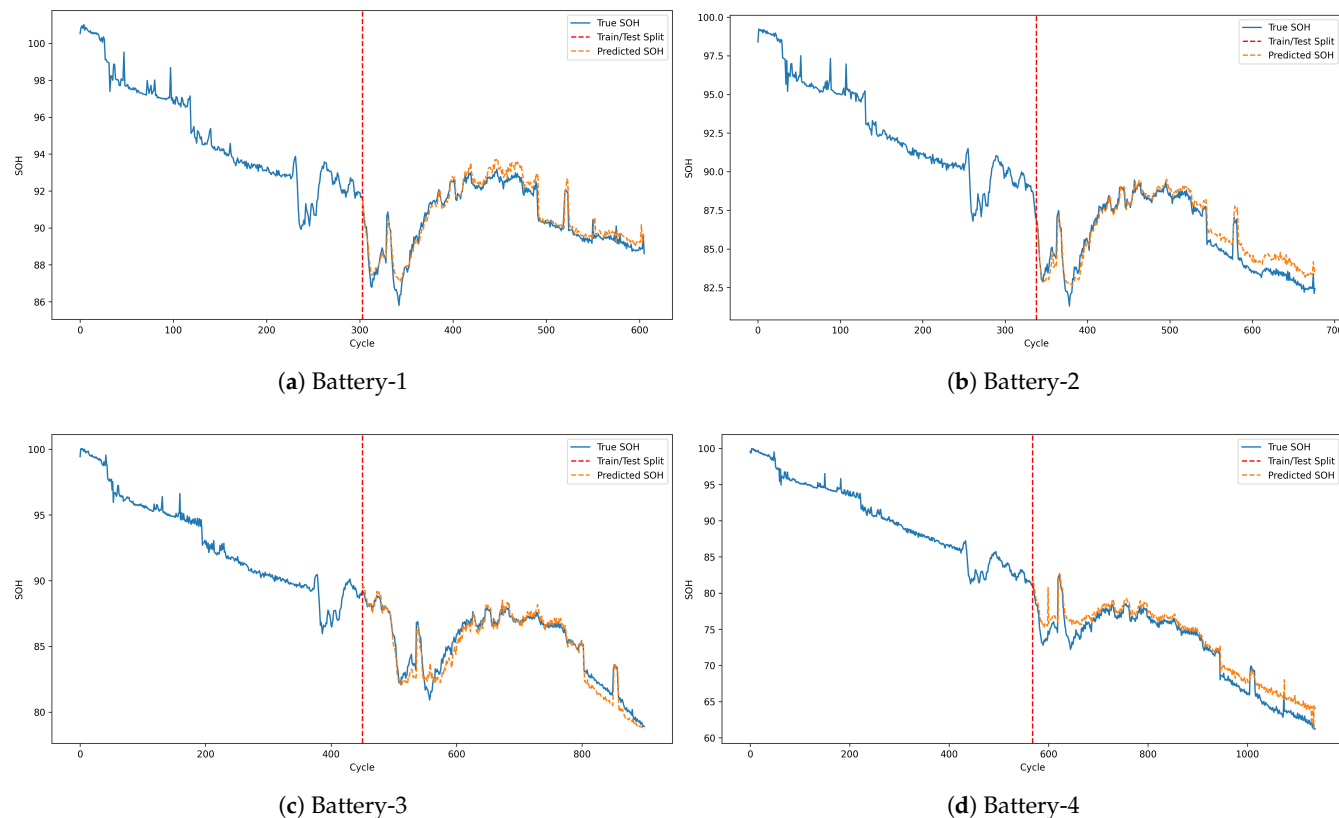
##### 5.5. The Influence of Temperature Characteristics

Figure 13 illustrates the variation of average temperature with battery charge-discharge cycles, while Figure 10 shows the change in battery SOH over the same cycles. Combining the two analyses reveals that as the average temperature decreases, the battery SOH also declines. This further demonstrates the significant impact of temperature on battery SOH.

To further study the impact of the temperature feature on the model's estimation accuracy, we retrained the model without the temperature feature and compared its performance to the model with the temperature feature. Removing the temperature component boosted the model's MAE and RMSE while decreasing  $R^2$ , indicating an increase in prediction error and a reduction in model performance. This result shows that temperature factors have a major influence on the model's predictability. Figure 14 shows the prediction results after removing the temperature feature. Table 8 summarizes the specific values of each performance metric for the model before and after removing the temperature feature.



**Figure 13.** The curve of average temperature versus the number of charging times.



**Figure 14.** Figure of the prediction results of the KAN-LSTM model under the condition of missing temperature features.

**Table 8.** Performance of KAN-LSTM estimation of SOH with missing temperature features.

Battery	MAE (%)	RMSE (%)	$R^2$ (%)
1	0.3351	0.4336	93.74
2	0.5794	0.6978	90.68
3	0.4579	0.6049	94.62
4	1.2559	1.5162	92.29

It is clear that the temperature feature helps to improve the model's accuracy and stability, as indicated by the drop in model performance when this element is eliminated.

### 5.6. Other Experimental Datasets

To test the model's generality and resilience, further experiments were conducted using datasets from other laboratories. Specifically, we utilized the lithium battery charge and discharge dataset provided by NASA [40]. This dataset contains charge and discharge cycle data for different lithium batteries under a variety of operating situations and is commonly used for predicting battery life and analyzing performance.

Three lithium-ion batteries, each charged in constant current (CC) mode at 1.5 A until the batteries' voltage reached 4.2 V and then in constant-voltage (CV) mode until the charging current decreased to 20 mA, were used to provide the charge and discharge data. The difference is in the discharge strategy: the batteries were drained at a constant current (CC) of 2 A until the voltages decreased to 2.7 V, 2.5 V, and 2.2 V, respectively. The three batteries in this investigation are labeled 5, 6, and 7, correspondingly.

During the experiment, we first preprocessed the NASA dataset to ensure that the format and characteristics of the data were consistent with those in our original experiments.

iment. We then applied the same model and approach, training and predicting on the NASA dataset.

The experimental results are shown in Figure 15, and the performance of the model on the NASA dataset is highly consistent with its performance on the original dataset, as reflected in key performance indicators such as MAE, RMSE, and  $R^2$ . Additionally, Table 9 provides a detailed summary of the model's performance indicators on the NASA datasets, clearly highlighting its predictive effectiveness across different datasets.

**Table 9.** Performance of KAN-LSTM for estimating SOH on NASA dataset.

Battery	MAE (%)	RMSE (%)	$R^2$ (%)
5	0.3841	0.5265	98.11
6	0.6062	0.8441	96.86
7	0.3161	0.4261	98.06

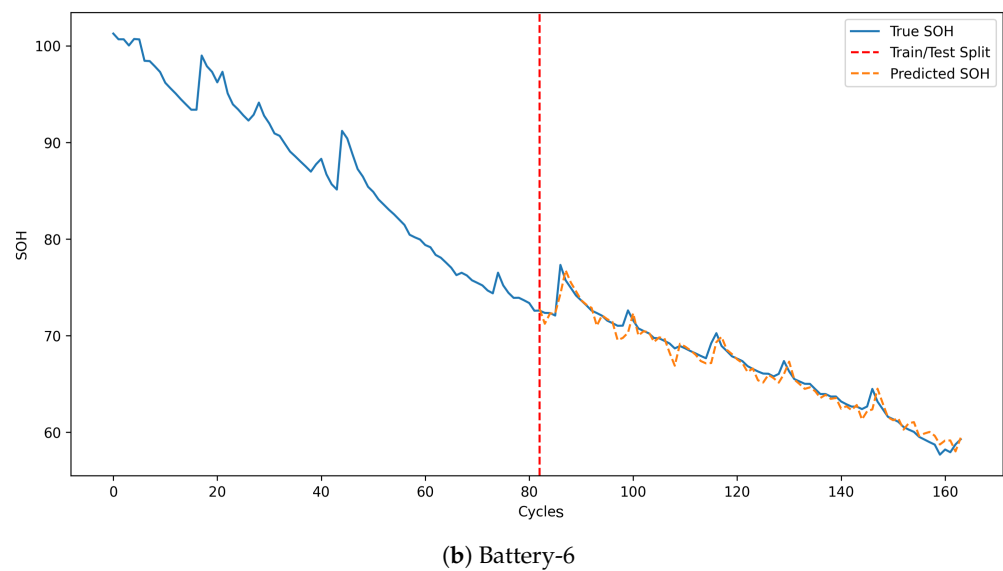
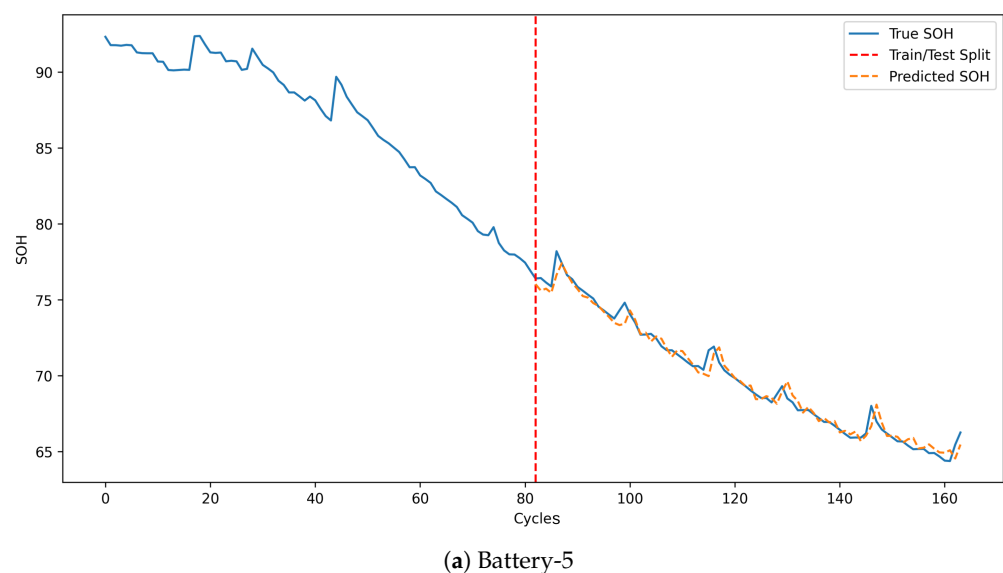


**Figure 15. Cont.**

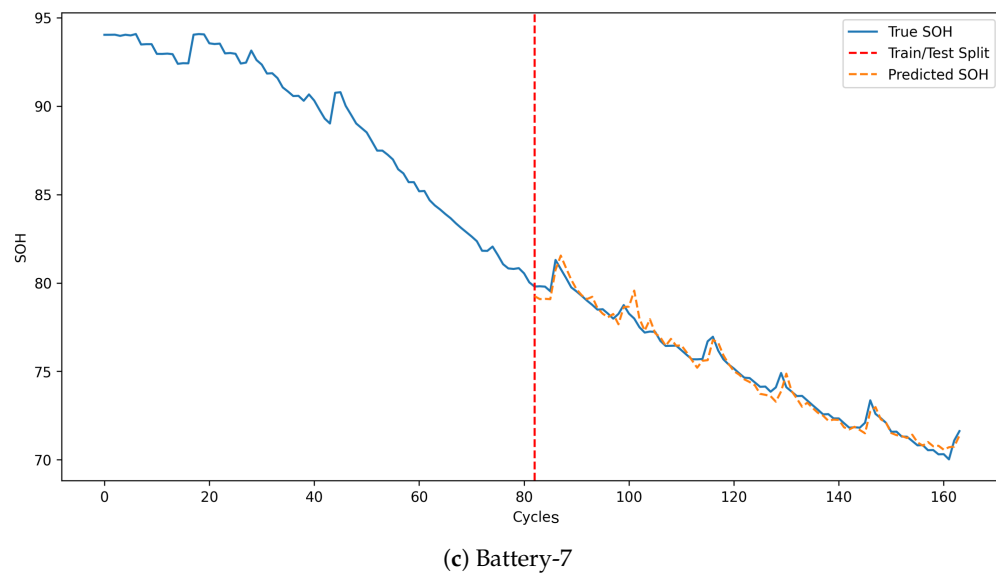


**Figure 15.** Model performance on the NASA dataset.

The data in the table shows that the model's performance across different datasets is relatively consistent. The MAE and RMSE indicators exhibit a small range of variation between the two datasets, and the  $R^2$  indicator also performs well on both datasets. This consistency further proves the model's robustness to differences in data, demonstrating its strong universality and stability.

## 5.7. Cross-Battery Prediction Experiments

In this experiment, we categorized the batteries into two groups based on their charging parameters. The first group consists of Battery 1 and Battery 2, both charged at a constant current rate of 0.1 C. For this group, we utilized the charge–discharge cycle data of Battery 1 as the training set and the corresponding data of Battery 2 as the validation set. The prediction results for this setup are shown in Figure 16a.

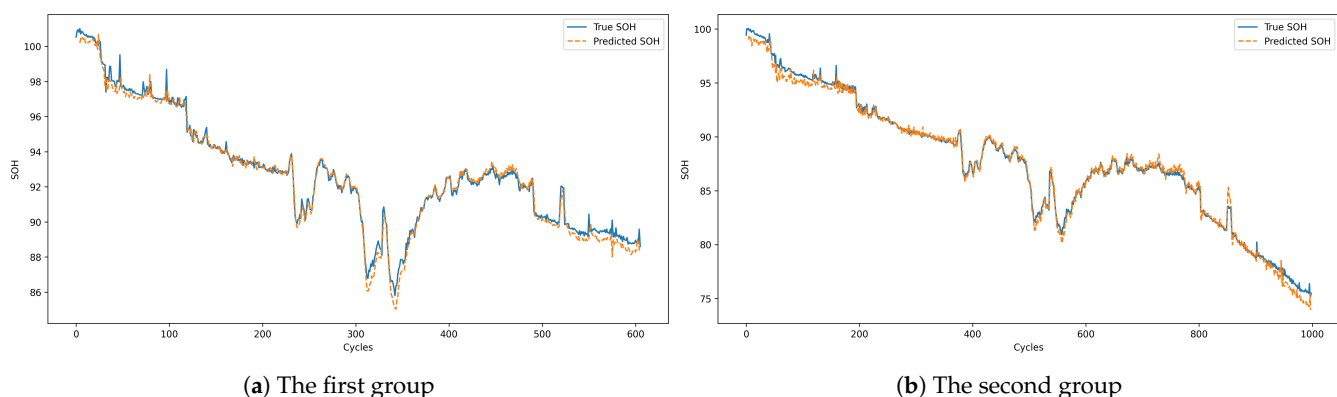


**Figure 16.** Prediction results across batteries at different charging rates.

The second group includes Battery 3 and Battery 4, which are both charged at a constant current rate of 0.2 C. In this case, the charge–discharge cycle data of Battery 3 was used for training, while Battery 4’s data served as the validation set. The prediction results for this configuration are illustrated in Figure 16b.

The evaluation results, summarized in Table 10, demonstrate robust predictive performance across both groups. The R-squared values consistently exceed 98%, indicating a strong correlation between the predicted and actual SOH values. Moreover, the MAE values are all below 0.2, and the RMSE values remain under 0.2, highlighting the accuracy

and reliability of the model in cross-battery prediction scenarios. These results underscore the model's capability to generalize effectively across different batteries with similar charging parameters.

**Table 10.** Performance Metrics for Cross-Battery SOH Prediction.

Group	MAE (%)	RMSE (%)	R <sup>2</sup> (%)
1	0.2847	0.3946	98.52
2	0.3602	0.4791	99.33

## 6. Conclusions

This study proposes a lithium-ion battery State of Health (SOH) prediction model based on multi-features and the KAN-LSTM framework, significantly improving SOH prediction accuracy. In the research, electrical and thermal features were extracted from the complete charging phase of lithium-ion batteries. The electrical features include constant-voltage charging time, the integral of current over time, and the chi-square statistic of current. These features provide an in-depth examination of the charging and discharging processes of lithium-ion batteries from the perspectives of dynamic changes and long-term cumulative effects. Through Pearson correlation analysis, we confirmed that these features exhibit strong correlations with battery SOH.

This study also investigates the impact of temperature variations on battery SOH estimation. Temperature changes across different seasons (temperature range of 10 °C to 30 °C) significantly influence battery capacity degradation, as detailed in Figures 10 and 13.

We proposed a high-performance KAN-LSTM model. Rigorous experimental validation was conducted on datasets with four different charging current rates. Even in scenarios where the battery SOH degradation process exhibits significant nonlinearity, the model achieved RMSEs of 0.29%, 0.37%, 0.43%, and 0.76%, and MAEs of 0.20%, 0.26%, 0.28%, and 0.57%, respectively. The model's average coefficient of determination ( $R^2$ ) reached 97.50%. Furthermore, experimental results across different batteries further validated the generalizability and robustness of the proposed model.

**Author Contributions:** Conceptualization, Z.Z., C.Z. and G.S.; Methodology, Z.Z., R.Z. and C.Z.; Software, R.Z., X.L. (Xin Liu) and Y.Z.; Validation, R.Z.; Formal analysis, Z.Z.; Investigation, Z.Z., R.Z., C.Z., Z.Y., X.L. (Xuming Liu) and S.C.; Writing—original draft, Z.Z. and R.Z.; Writing—review & editing, Z.Z.; Visualization, R.Z., X.L. (Xin Liu), Y.Z., X.L. (Xuming Liu), S.C., X.D., P.J. and Z.S.; Supervision, Z.Z. and C.Z.; Project administration, Z.Z.; Funding acquisition, Z.Z. All authors have read and agreed to the published version of the manuscript.

**Funding:** This work was supported by the scientific research foundation for high-level personnel in Jinling Institute of Technology (jit-b-201811) and the Industry-University-Research Cooperation Project of Jiangsu Province (BY2021300).

**Data Availability Statement:** The original contributions presented in the study are included in the article, further inquiries can be directed to the corresponding authors.

**Conflicts of Interest:** The authors declare no conflicts of interest.

## References

1. Rui, X.; Li, L.; Tian, J. Towards a smarter battery management system: A critical review on battery state of health monitoring methods. *J. Power Sources* **2018**, *405*, 18–29.
2. Anna, M.; Uebel, M.; Rohwerder, M. The protection zone: A long-range corrosion protection mechanism around conducting polymer particles in composite coatings: Part I. polyaniline and polypyrrole. *J. Electrochem. Soc.* **2019**, *166*, C304.
3. Rui, X.; Wang, J.; Shen, W.; Tian, J.; Mu, H. Co-estimation of state of charge and capacity for lithium-ion batteries with multi-stage model fusion method. *Engineering* **2021**, *7*, 1469–1482.
4. Yu, Q.; Nie, Y.; Peng, S.; Miao, Y.; Zhai, C.; Zhang, R.; Han, J.; Zhao, S.; Pecht, M. Evaluation of the safety standards system of power batteries for electric vehicles in China. *Appl. Energy* **2023**, *349*, 121674. [CrossRef]
5. Kuo, S.; Ni, H.; Fan, L. Flexible graphene-based composite films for supercapacitors with tunable areal capacitance. *Electrochim. Acta* **2017**, *235*, 233–241.

6. Wang, Y.; Tian, J.; Sun, Z.; Wang, L.; Xu, R.; Li, M.; Chen, Z. A comprehensive review of battery modeling and state estimation approaches for advanced battery management systems. *Renew. Sustain. Energy Rev.* **2020**, *131*, 110015. [[CrossRef](#)]
7. Zhang, C.; Zhao, S.; Yang, Z.; He, Y. A multi-fault diagnosis method for lithium-ion battery pack using curvilinear Manhattan distance evaluation and voltage difference analysis. *J. Energy Storage* **2023**, *67*, 107575. [[CrossRef](#)]
8. Lu, L.; Han, X.; Li, J.; Hua, J.; Ouyang, M. A review on the key issues for lithium-ion battery management in electric vehicles. *J. Power Sources* **2013**, *226*, 272–288. [[CrossRef](#)]
9. Amir, S.; Gulzar, M.; Tarar, M.O.; Naqvi, I.H.; Zaffar, N.A.; Pecht, G.M. Dynamic equivalent circuit model to estimate state-of-health of lithium-ion batteries. *IEEE Access* **2022**, *10*, 18279–18288. [[CrossRef](#)]
10. Tran, M.-K.; Mathew, M.; Janhunen, S.; Panchal, S.; Raahemifar, K.; Fraser, R.; Fowler, M. A comprehensive equivalent circuit model for lithium-ion batteries, incorporating the effects of state of health, state of charge, and temperature on model parameters. *J. Energy Storage* **2021**, *43*, 103252. [[CrossRef](#)]
11. Xiong, R.; Li, L.; Li, Z.; Yu, Q.; Mu, H. An electrochemical model based degradation state identification method of Lithium-ion battery for all-climate electric vehicles application. *Appl. Energy* **2018**, *219*, 264–275. [[CrossRef](#)]
12. Li, J.; Adewuyi, K.; Lotfi, N.; Landers, R.G.; Park, J. A single particle model with chemical/mechanical degradation physics for lithium ion battery State of Health (SOH) estimation. *Appl. Energy* **2018**, *212*, 1178–1190. [[CrossRef](#)]
13. Yang, S.; Zhang, C.; Jiang, J.; Zhang, W.; Gao, Y.; Zhang, L. A voltage reconstruction model based on partial charging curve for state-of-health estimation of lithium-ion batteries. *J. Energy Storage* **2021**, *35*, 102271. [[CrossRef](#)]
14. Zheng, Y.; Cui, Y.; Han, X.; Ouyang, M. A capacity prediction framework for lithium-ion batteries using fusion prediction of empirical model and data-driven method. *Energy* **2021**, *237*, 121556. [[CrossRef](#)]
15. Chen, L.; Xie, S.; Lopes, A.M.; Li, H.; Bao, X.; Zhang, C.; Li, P. A new SOH estimation method for Lithium-ion batteries based on model-data-fusion. *Energy* **2024**, *286*, 129597. [[CrossRef](#)]
16. Wang, Z.; Yuan, C.; Li, X. Lithium battery state-of-health estimation via differential thermal voltammetry with Gaussian process regression. *IEEE Trans. Transp. Electrif.* **2020**, *7*, 16–25. [[CrossRef](#)]
17. Li, R.; Li, W.; Zhang, H. State of Health and Charge Estimation Based on Adaptive Boosting integrated with particle swarm optimization/support vector machine (AdaBoost-PSO-SVM) Model for Lithium-ion Batteries. *Int. J. Electrochem. Sci.* **2022**, *17*, 220212. [[CrossRef](#)]
18. Deng, Z.; Hu, X.; Li, P.; Lin, X.; Bian, X. Data-driven battery state of health estimation based on random partial charging data. *IEEE Trans. Power Electron.* **2021**, *37*, 5021–5031. [[CrossRef](#)]
19. Zhang, C.; Zhao, S.; Yang, Z.; Chen, Y. A reliable data-driven state-of-health estimation model for lithium-ion batteries in electric vehicles. *Front. Energy Res.* **2022**, *10*, 1013800. [[CrossRef](#)]
20. Bao, X.; Chen, L.; Lopes, A.M.; Li, X.; Xie, S.; Li, P.; Chen, Y. Hybrid deep neural network with dimension attention for state-of-health estimation of lithium-ion batteries. *Energy* **2023**, *278*, 127734. [[CrossRef](#)]
21. Liu, Y.; Sun, J.; Shang, Y.; Zhang, X.; Ren, S.; Wang, D. A novel remaining useful life prediction method for lithium-ion battery based on long short-term memory network optimized by improved sparrow search algorithm. *J. Energy Storage* **2023**, *61*, 106645. [[CrossRef](#)]
22. Van, C.N.; Quang, D.T. Estimation of SoH and internal resistances of Lithium ion battery based on LSTM network. *Int. J. Electrochem. Sci.* **2023**, *18*, 100166.
23. Tang, A.; Jiang, Y.; Yu, Q.; Zhang, Z. A hybrid neural network model with attention mechanism for state of health estimation of lithium-ion batteries. *J. Energy Storage* **2023**, *68*, 107734. [[CrossRef](#)]
24. Zhang, C.; Luo, L.; Yang, Z.; Du, B.; Zhou, Z.; Wu, J.; Chen, L. Flexible method for estimating the state of health of lithium-ion batteries using partial charging segments. *Energy* **2024**, *295*, 131009. [[CrossRef](#)]
25. Fan, Y.; Xiao, F.; Li, C.; Yang, G.; Tang, X. A novel deep learning framework for state of health estimation of lithium-ion battery. *J. Energy Storage* **2020**, *32*, 101741. [[CrossRef](#)]
26. Yang, K.; Tang, Y.; Zhang, S.; Zhang, Z. A deep learning approach to state of charge estimation of lithium-ion batteries based on dual-stage attention mechanism. *Energy* **2022**, *244*, 123233. [[CrossRef](#)]
27. Li, H.; Fu, L.; Long, X.; Liu, L.; Zeng, Z. A hybrid deep learning model for lithium-ion batteries state of charge estimation based on quantile regression and attention. *Energy* **2024**, *294*, 130834. [[CrossRef](#)]
28. Jiang, B.; Dai, H.; Wei, X.; Jiang, Z. Multi-kernel relevance vector machine with parameter optimization for cycling aging prediction of lithium-ion batteries. *IEEE J. Emerg. Sel. Top. Power Electron.* **2021**, *11*, 175–186. [[CrossRef](#)]
29. Li, X.; Ma, X.; Xiao, F.; Xiao, C.; Wang, F.; Zhang, S. Time-series production forecasting method based on the integration of Bidirectional Gated Recurrent Unit (Bi-GRU) network and Sparrow Search Algorithm (SSA). *J. Pet. Sci. Eng.* **2022**, *208*, 109309. [[CrossRef](#)]
30. Wu, J.; Cui, X.; Meng, J.; Peng, J.; Lin, M. Data-driven transfer-stacking-based state of health estimation for lithium-ion batteries. *IEEE Trans. Ind. Electron.* **2023**, *71*, 604–614. [[CrossRef](#)]
31. Wang, J.; Zhang, C.; Meng, X.; Zhang, L.; Li, X.; Zhang, W. A Novel Feature Engineering-Based SOH Estimation Method for Lithium-Ion Battery with Downgraded Laboratory Data. *Batteries* **2024**, *10*, 139. [[CrossRef](#)]
32. Xu, H.; Wu, L.; Xiong, S.; Li, W.; Garg, A.; Gao, L. An improved CNN-LSTM model-based state-of-health estimation approach for lithium-ion batteries. *Energy* **2023**, *276*, 127585. [[CrossRef](#)]

33. Wen, J.; Chen, X.; Li, X.; Li, Y. SOH prediction of lithium battery based on IC curve feature and BP neural network. *Energy* **2022**, *261*, 125234. [[CrossRef](#)]
34. Chen, Z.; Zhao, H.; Zhang, Y.; Shen, S.; Shen, J.; Liu, Y. State of health estimation for lithium-ion batteries based on temperature prediction and gated recurrent unit neural network. *J. Power Sources* **2022**, *521*, 230892. [[CrossRef](#)]
35. Lin, C.; Xu, J.; Shi, M.; Mei, X. Constant current charging time based fast state-of-health estimation for lithium-ion batteries. *Energy* **2022**, *247*, 123556. [[CrossRef](#)]
36. Zhang, C.; Luo, L.; Yang, Z.; Zhao, S.; He, Y.; Wang, X.; Wang, H. Battery SOH estimation method based on gradual decreasing current, double correlation analysis and GRU. *Green Energy Intell. Transp.* **2023**, *2*, 100108. [[CrossRef](#)]
37. Cao, T.; Xu, Y.; Liu, G.; Tao, S.; Tang, W.; Sun, H. Feature-enhanced deep learning method for electric vehicle charging demand probabilistic forecasting of charging station. *Appl. Energy* **2024**, *371*, 123751. [[CrossRef](#)]
38. Pepe, S.; Ciucci, F. Long-range battery state-of-health and end-of-life prediction with neural networks and feature engineering. *Appl. Energy* **2023**, *350*, 121761. [[CrossRef](#)]
39. Peng, S.; Zhu, J.; Wu, T.; Tang, A.; Kan, J.; Pecht, M. SOH early prediction of Lithium-ion batteries based on voltage interval selection and features fusion. *Energy* **2024**, *308*, 132993. [[CrossRef](#)]
40. Chen, D.; Hong, W.; Zhou, X. Transformer network for remaining useful life prediction of lithium-ion batteries. *IEEE Access* **2022**, *10*, 19621–19628. [[CrossRef](#)]

**Disclaimer/Publisher’s Note:** The statements, opinions and data contained in all publications are solely those of the individual author(s) and contributor(s) and not of MDPI and/or the editor(s). MDPI and/or the editor(s) disclaim responsibility for any injury to people or property resulting from any ideas, methods, instructions or products referred to in the content.